

# HYPERELLIPTIC THETA-FUNCTIONS AND SPECTRAL METHODS

J. FRAUENDIENER AND C. KLEIN

**ABSTRACT.** A code for the numerical evaluation of hyperelliptic theta-functions is presented. Characteristic quantities of the underlying Riemann surface such as its periods are determined with the help of spectral methods. The code is optimized for solutions of the Ernst equation where the branch points of the Riemann surface are parameterized by the physical coordinates. An exploration of the whole parameter space of the solution is thus only possible with an efficient code. The use of spectral approximations allows for an efficient calculation of all quantities in the solution with high precision. The case of almost degenerate Riemann surfaces is addressed. Tests of the numerics using identities for periods on the Riemann surface and integral identities for the Ernst potential and its derivatives are performed. It is shown that an accuracy of the order of machine precision can be achieved. These accurate solutions are used to provide boundary conditions for a code which solves the axisymmetric stationary Einstein equations. The resulting solution agrees with the theta-functional solution to very high precision.

## 1. INTRODUCTION

Solutions to integrable differential equations in terms of theta-functions were introduced with the works of Novikov, Dubrovin, Matveev, Its, Krichever, ... (see [7, 19, 28, 2]) for the Korteweg-de Vries (KdV) equation. Such solutions to e.g. the KdV, the Sine-Gordon, and the Non-linear Schrödinger equation describe periodic or quasi-periodic solutions, see [8, 2]. They are given explicitly in terms of Riemann theta-functions defined on some Riemann surface. Though all quantities entering the solution are in general given in explicit form via integrals on the Riemann surface, the work with theta-functional solutions admittedly has not reached the importance of soliton solutions.

The main reason for the more widespread use of solitons is that they are given in terms of algebraic or exponential functions. On the other hand the parameterization of theta-functions by the underlying Riemann surface is very implicit. The main parameters, typically the branch points of the Riemann surface, enter the solutions as parameters in integrals on the Riemann surface. A full understanding of the functional dependence on these parameters seems to be only possible numerically. In recent years algorithms have been developed to establish such relations for rather general Riemann surfaces as in [33] or via Schottky uniformization (see [2]), which have been incorporated successively in numerical and symbolic codes, see [32, 18, 14, 5, 6] and references therein (the last two references are distributed along with Maple 6, respectively Maple 8, and as a Java implementation at [36]). For an approach to express periods of hyperelliptic Riemann surfaces via theta constants see [9].

---

*Date:* February 4, 2008.

*Key words and phrases.* hyperelliptic theta-functions, spectral methods.

These codes are convenient to study theta-functional solutions of equations of KdV-type where the considered Riemann surfaces are ‘static’, i.e., independent of the physical coordinates. In these cases the characteristic quantities of the Riemann surface have to be calculated once, just the comparatively fast summation in the approximation of the theta series via a finite sum as e.g. in [6] has to be carried out in dependence of the space-time coordinates.

The purpose of this article is to study numerically theta-functional solutions of the Ernst equation [10] which were given by Korotkin [25]. In this case the branch points of the underlying hyperelliptic Riemann surface are parameterized by the physical coordinates, the spectral curve of the Ernst equation is in this sense ‘dynamical’. The solutions are thus not studied on a single Riemann surface but on a whole family of surfaces. This implies that the time-consuming calculation of the periods of the Riemann surface has to be carried out for each point in the space-time. This includes limiting cases where the surface is almost degenerate. In addition the theta-functional solutions should be calculated to high precision in order to be able to test numerical solutions for rapidly rotating neutron stars such as provided e.g. by the spectral code LORENE [35]. This requires a very efficient code of high precision.

We present here a numerical code for hyperelliptic surfaces where the integrals entering the solution are calculated by expanding the integrands with a Fast Cosine Transformation in MATLAB. The precision of the numerical evaluation is tested by checking identities for periods on Riemann surfaces and by comparison with exact solutions. The code is in principle able to deal with general (non-singular) hyperelliptic surfaces, but is optimized for a genus 2 solution to the Ernst equation which was constructed in [22, 23]. We show that an accuracy of the order of machine precision ( $\sim 10^{-14}$ ) can be achieved at a space-time point in general position with 32 polynomials and in the case of almost degenerate surfaces which occurs e.g., when the point approaches the symmetry axis with at most 256 polynomials. Global tests of the numerical accuracy of the solutions to the Ernst equation are provided by integral identities for the Ernst potential and its derivatives: the equality of the Arnowitt-Deser-Misner (ADM) mass and the Komar mass (see [24, 34]) and a generalization of the Newtonian virial theorem as derived in [15]. We use the so determined numerical data for the theta-functions to provide ‘exact’ boundary values on a sphere for the program library LORENE [35] which was developed for a numerical treatment of rapidly rotating neutron stars. LORENE solves the boundary value problem for the stationary axisymmetric Einstein equations with spectral methods. We show that the theta-functional solution is reproduced to the order of  $10^{-11}$  and better.

The paper is organized as follows: in section 2 we collect useful facts on the Ernst equation and hyperelliptic Riemann surfaces, in section 3 we summarize basic features of spectral methods and explain our implementation of various quantities. The calculation of the periods of the hyperelliptic surface and the non-Abelian line integrals entering the solution is performed together with tests of the precision of the numerics. In section 4 we check integral identities for the Ernst potential. The test of the spectral code LORENE is presented in section 5. In section 6 we add some concluding remarks.

## 2. ERNST EQUATION AND HYPERELLIPTIC RIEMANN SURFACES

The Ernst equation for the complex valued potential  $\mathcal{E}$  (we denote the real and the imaginary part of  $\mathcal{E}$  with  $f$  and  $b$  respectively) depending on the two coordinates

$(\rho, \zeta)$  can be written in the form

$$(1) \quad \Re \mathcal{E} \left( \mathcal{E}_{\rho\rho} + \frac{1}{\rho} \mathcal{E}_\rho + \mathcal{E}_{\zeta\zeta} \right) = \mathcal{E}_\rho^2 + \mathcal{E}_\zeta^2.$$

The equation has a physical interpretation as the stationary axisymmetric Einstein equations in vacuum (see appendix and references given therein). Its complete integrability was shown by Maison [29] and Belinski-Zakharov [1]. For real Ernst potential, the Ernst equation reduces to the axisymmetric Laplace equation for  $\ln \mathcal{E}$ . The corresponding solutions are static and belong to the so called Weyl class, see [27].

Algebro-geometric solutions to the Ernst equation were given by Korotkin [25]. The solutions are defined on a family of hyperelliptic surfaces  $\mathcal{L}(\xi, \bar{\xi})$  with  $\xi = \zeta - i\rho$  corresponding to the plane algebraic curve

$$(2) \quad \mu^2 = (K - \xi)(K - \bar{\xi}) \prod_{i=1}^g (K - E_i)(K - F_i),$$

where  $g$  is the genus of the surface and where the branch points  $E_i, F_i$  are independent of the physical coordinates and for each  $n$  subject to the reality condition  $E_n = \bar{F}_n$  or  $E_n, F_n \in \mathbb{R}$ .

Hyperelliptic Riemann surfaces are important since they show up in the context of algebro-geometric solutions of various integrable equations as KdV, Sine-Gordon and Ernst. Whereas it is a non-trivial problem to find a basis for the holomorphic differentials on general surfaces (see e.g. [5]), it is given in the hyperelliptic case (see e.g. [2]) by

$$(3) \quad d\nu_k = \left( \frac{dK}{\mu}, \frac{K dK}{\mu}, \dots, \frac{K^{g-1} dK}{\mu} \right),$$

which is the main simplification in the use of these surfaces. We introduce on  $\mathcal{L}$  a canonical basis of cycles  $(a_k, b_k)$ ,  $k = 1, \dots, n$ . The holomorphic differentials  $d\omega_k$  are normalized by the condition on the  $a$ -periods

$$(4) \quad \int_{a_l} d\omega_k = 2\pi i \delta_{lk}.$$

The matrix of  $b$ -periods is given by  $\mathbf{B}_{ik} = \int_{b_i} d\omega_k$ . The matrix  $\mathbf{B}$  is a so-called Riemann matrix, i.e. it is symmetric and has a negative definite real part. The Abel map  $\omega : \mathcal{L} \rightarrow \text{Jac}(\mathcal{L})$  with base point  $E_1$  is defined as  $\omega(P) = \int_{E_1}^P d\omega_k$ , where  $\text{Jac}(\mathcal{L})$  is the Jacobian of  $\mathcal{L}$ . The theta-function with characteristics corresponding to the curve  $\mathcal{L}$  is given by

$$(5) \quad \Theta_{\mathbf{p}\mathbf{q}}(\mathbf{x}|\mathbf{B}) = \sum_{\mathbf{n} \in \mathbb{Z}^g} \exp \left\{ \frac{1}{2} \langle \mathbf{B}(\mathbf{p} + \mathbf{n}), (\mathbf{p} + \mathbf{n}) \rangle + \langle \mathbf{p} + \mathbf{n}, 2i\pi\mathbf{q} + \mathbf{x} \rangle \right\},$$

where  $\mathbf{x} \in \mathbb{C}^g$  is the argument and  $\mathbf{p}, \mathbf{q} \in \mathbb{C}^g$  are the characteristics. We will only consider half-integer characteristics in the following. The theta-function with characteristics is, up to an exponential factor, equivalent to the theta-function with zero characteristic (the Riemann theta-function is denoted with  $\Theta$ ) and shifted argument,

$$(6) \quad \Theta_{\mathbf{p}\mathbf{q}}(\mathbf{x}|\mathbf{B}) = \Theta(\mathbf{x} + \mathbf{B}\mathbf{p} + 2i\pi\mathbf{q}) \exp \left\{ \frac{1}{2} \langle \mathbf{B}\mathbf{p}, \mathbf{p} \rangle + \langle \mathbf{p}, 2i\pi\mathbf{q} + \mathbf{x} \rangle \right\}.$$

We denote by  $d\omega_{PQ}$  a differential of the third kind, i.e., a 1-form which has poles in  $P, Q \in \mathcal{L}$  with respective residues  $+1$  and  $-1$ . This singularity structure characterizes the differentials only up to an arbitrary linear combination of holomorphic

differentials. The meromorphic differentials can be normalized by the condition that all  $a$ -periods vanish. We use the notation  $\infty^\pm$  for the infinite points on different sheets of the curve  $\mathcal{L}$ , namely  $\mu/K^{g+1} \rightarrow \pm 1$  as  $K \rightarrow \infty^\pm$ . The differential  $d\omega_{\infty^+ \infty^-}$  is given up to holomorphic differentials by  $-K^g dK/\mu$ . It is well known that the  $b$ -periods of normalized differentials of the third kind can be expressed in terms of the Abel map (see e.g. [8]),

$$(7) \quad \int_{b_k} d\omega_{PQ} = \omega_k(P) - \omega_k(Q), \quad k = 1, \dots, g.$$

In [20, 21] a physically interesting subclass of Korotkin's solution was identified which can be written in the form

$$(8) \quad \mathcal{E} = \frac{\Theta_{\mathbf{p}\mathbf{q}}(\omega(\infty^+) + \mathbf{u})}{\Theta_{\mathbf{p}\mathbf{q}}(\omega(\infty^-) + \mathbf{u})} \cdot e^I,$$

where  $\mathbf{u} = (u_k) \in \mathbb{C}^g$  and where

$$(9) \quad I = \frac{1}{2\pi i} \int_{\Gamma} \ln G(K) d\omega_{\infty^+ \infty^-}(K), \quad u_k = \frac{1}{2\pi i} \int_{\Gamma} \ln G(K) d\omega_k.$$

$\Gamma$  is a piece-wise smooth contour on  $\mathcal{L}$  and  $G(K)$  is a non-zero Hölder-continuous function on  $\Gamma$ . The contour  $\Gamma$  and the function  $G$  have to satisfy the reality conditions that with  $K \in \Gamma$  also  $\bar{K} \in \Gamma$  and  $\bar{G}(\bar{K}) = G(K)$ ; both are independent of the physical coordinates.

In the following we will discuss the example of the solution constructed in [22, 23] which can be interpreted as a disk of collisionless matter. For a physical interpretation see [13]. The solution is given on a surface of the form (2) with genus 2. The branch points independent of the physical coordinates are related through the relations  $E_i = \bar{F}_i$ ,  $i = 1, 2$  and  $E_1 = -F_2$ . The branch points are parameterized by two real parameters  $\lambda$  and  $\delta$ . Writing  $E_1^2 = \alpha + i\beta$  with real  $\alpha, \beta$ , we have

$$(10) \quad \alpha = -1 + \frac{\delta}{2}, \quad \beta = \sqrt{\frac{1}{\lambda^2} + \delta - \frac{\delta^2}{4}}.$$

The contour  $\Gamma$  is the piece of the covering of the imaginary axis in the upper sheet between  $[-i, i]$ , the function  $G$  has the form

$$(11) \quad G(K) = \frac{\sqrt{(K^2 - \alpha)^2 + \beta^2} + K^2 + 1}{\sqrt{(K^2 - \alpha)^2 + \beta^2} - K^2 - 1}.$$

The physical parameters vary between  $\delta = 0$ , the solution which was first given in [30], and  $\delta_s = 2(1 + \sqrt{1 + 1/\lambda^2})$ , the static limit in which  $\beta = 0$ . In the latter case the Riemann surface degenerates, the resulting Ernst potential (8) is real and be expressed in terms of objects corresponding to the surface  $\mathcal{L}_0$  of genus 0 defined by the relation  $\mu_0^2 = (K - \xi)(K - \bar{\xi})$ . The parameter  $\lambda$  varies between  $\lambda = 0$ , the so-called Newtonian limit where the branch points  $E_i, F_i$  tend to infinity. Since  $G$  is also of order  $\lambda$  in this limit, the lowest order contributions are again real and defined on the surface  $\mathcal{L}_0$ . This case corresponds to the disk limit of the Maclaurin ellipsoids, see [3]. The upper limit for  $\lambda$  is infinity for  $\delta \neq 0$  and  $\lambda_c = 4.629 \dots$  for  $\delta = 0$ . The limiting situation is special in the second case since the resulting spacetime is no longer asymptotically flat and since the axis is singular. The invariant circumference of the disk is zero in this case which implies that the disk shrinks to a point for an observer in the exterior of the disk, see [13].

For physical reasons the solution was discussed in [13] in dependence of two other real parameters  $\epsilon$  and  $\gamma$ . Here  $\epsilon$  is related to the redshift of photons emitted at the center of the disk and detected at infinity. It varies between 0 in the Newtonian limit, and 1 in the ultra-relativistic limit, where photons cannot escape to infinity.

Thus,  $\epsilon$  is a measure of how relativistic the situation is. The parameter  $\gamma$  is a measure of how static the solution is, it varies between 0, indicating the static limit and 1. For the functional relations between  $\epsilon$ ,  $\gamma$  and  $\lambda$ ,  $\delta$  see [13]. The constant  $\Omega$  (with respect to the physical coordinates) to appear in the following can be considered as a natural scale for the angular velocities in the disk, for a definition see [13].

The coordinate  $\rho$  can take all non-negative real values, the coordinate  $\zeta$  all real values. The example we are studying here has an equatorial symmetry,

$$(12) \quad \mathcal{E}(\rho, -\zeta) = \bar{\mathcal{E}}(\rho, \zeta).$$

It is therefore sufficient to consider only non-negative values of  $\zeta$ . The case  $\rho = 0$  corresponds to the axis of symmetry where the branch cut  $[\xi, \bar{\xi}]$  degenerates to a point. As was shown in [21, 13], the Ernst potential can be written in this limit in terms of theta-functions on the elliptic surface  $\mathcal{L}_1$  defined by  $\mu_1^2 = (K^2 - \alpha)^2 + \beta^2$ , i.e. the surface  $\mathcal{L}$  with the cut  $[\xi, \bar{\xi}]$  removed. Near the axis the Ernst potential has the form (see [11, 21])

$$(13) \quad \mathcal{E}(\rho, \zeta) = \mathcal{E}_0(\zeta) + \rho^2 \mathcal{E}_1(\zeta) + \mathcal{O}(\rho^4);$$

here  $\mathcal{E}_0$  and  $\mathcal{E}_1$  are independent of  $\rho$ ,  $\mathcal{E}_0$  is the axis potential. This formula could be used to calculate the potential close to the axis. However we considered only values of  $\rho$  greater than  $10^{-5}$  and did not experience any numerical problems. Consequently we did not use formula (13).

For large values of  $r = |\xi|$ , the Ernst potential has the asymptotic expansion

$$(14) \quad \mathcal{E} = 1 - \frac{2m}{r} + \frac{2m^2}{r^2} - \frac{2iJ\zeta}{r^3} + \mathcal{O}(1/r^3);$$

here the constants (with respect to  $\xi$ )  $m$  and  $J$  are the ADM-mass and, respectively, the angular momentum of the space-time. They can be calculated on the axis in terms of elliptic theta-functions, see [13]. Formula (14) is used for values of  $r > 10^6$ .

In the limit  $\xi = E_2$ , the Ernst potential can be given on the surface  $\Sigma_0$  of genus 0 obtained by removing the cuts  $[\xi, \bar{\xi}]$  and  $[E_2, F_2]$  from the surface  $\mathcal{L}$ . The potential can thus be given in this case in terms of elementary functions, see [13].

In the equatorial plane  $\zeta = 0$ , the Riemann surface  $\mathcal{L}$  has an additional involution  $K \rightarrow -K$  as can be seen from (2). This implies that the surface can be considered as a covering of an elliptic surface, see [2, 21]. The theta-functions in (8) can be written as sums of theta-functions on the covered surface and on the Prym variety which happens to be an elliptic surface as well in this case. We use this fact at the disk ( $\zeta = 0$ ,  $\rho \leq 1$ ), where the moving branch points are situated on  $\Gamma$ . There all quantities can be expressed in terms of quantities defined on the Prym surface  $\Sigma_w$  defined by  $\mu_w^2 = (K + \rho^2)((K - \alpha)^2 + \beta^2)$ , see [13].

### 3. NUMERICAL IMPLEMENTATIONS

The numerical task in this work is to approximate and evaluate analytically defined functions as accurately and efficiently as possible. To this end it is advantageous to use (pseudo-)spectral methods which are distinguished by their excellent approximation properties when applied to smooth functions. Here the functions are known to be analytic except for isolated points. In this section we explain the basic ideas behind the use of spectral methods and describe in detail how the theta-functions and the Ernst potential can be obtained to a high degree of accuracy.

**3.1. Spectral approximation.** The basic idea of spectral methods is to approximate a given function  $f$  globally on its domain of definition by a linear combination

$$f \approx \sum_{k=0}^N a_k \phi_k,$$

where the function  $\phi_k$  are taken from some class of functions which is chosen appropriately for the problem at hand.

The coefficients  $a_k$  are determined by requiring that the linear combination should be ‘close’ to  $f$ . Thus, one could require that  $\|f - \sum_{k=0}^N a_k \phi_k\|$  should be minimal for some norm. Another possibility is to require that  $\langle f - \sum_{k=0}^N a_k \phi_k, \chi_l \rangle = 0$  for  $l = 0 : N$  with an appropriate inner product and associated orthonormal basis  $\chi_l$ . This is called the Galerkin method. Finally, one can demand that  $f(x_l) = \sum_{k=0}^N a_k \phi_k(x_l)$  at selected points  $(x_l)_{l=0:N}$ . This is the so called collocation method which is the one we will use in this paper. In this case the function values  $f_l = f(x_l)$  and the coefficients  $a_k$  are related by the matrix  $\Phi_{lk} = \phi_k(x_l)$ .

The choice of the expansion basis depends to a large extent on the specific problem. For periodic functions there is the obvious choice of trigonometric polynomials  $\phi_k(x) = \exp(2\pi i k/N)$  while for functions defined on a finite interval the most used functions are orthogonal polynomials, in particular Chebyshev and Legendre polynomials. While the latter are important because of their relationship with the spherical harmonics on the sphere, the former are used because they have very good approximation properties and because one can use fast transform methods when computing the expansion coefficients from the function values provided one chooses the collocation points  $x_l = \cos(\pi l/N)$  (see [12] and references therein). We will use here collocation with Chebyshev polynomials.

Let us briefly summarize here their basic properties. The Chebyshev polynomials  $T_n(x)$  are defined on the interval  $I = [-1, 1]$  by the relation

$$T_n(\cos(t)) = \cos(nt), \text{ where } x = \cos(t), \quad t \in [0, \pi].$$

They satisfy the differential equation

$$(15) \quad (1 - x^2) \phi''(x) - x\phi'(x) + n^2 \phi(x) = 0.$$

The addition theorems for sine and cosine imply the recursion relations

$$(16) \quad T_{n+1}(x) - 2x T_n(x) + T_{n-1}(x) = 0,$$

for the polynomials  $T_n$  and

$$(17) \quad \frac{T'_{n+1}(x)}{n+1} - \frac{T'_{n-1}(x)}{n-1} = 2T_n(x)$$

for their derivatives. The Chebyshev polynomials are orthogonal on  $I$  with respect to the hermitian inner product

$$\langle f, g \rangle = \int_{-1}^1 f(x) \bar{g}(x) \frac{dx}{\sqrt{1-x^2}}.$$

We have

$$(18) \quad \langle T_m, T_n \rangle = c_m \frac{\pi}{2} \delta_{mn}$$

where  $c_0 = 2$  and  $c_l = 1$  otherwise.

Now suppose that a function  $f$  on  $I$  is sampled at the points  $x_l = \cos(\pi l/N)$  and that  $\sum_{n=0}^N a_n T_n$  is the interpolating polynomial. Defining  $c_0 = c_N = 2$ ,  $c_n = 1$  for

$0 < n < N$  in the discrete case and the numbers  $F_n = c_n a_n$  we have

$$\begin{aligned} f_l &= \sum_{n=0}^N a_n T_n(x_l) = \sum_{n=0}^N a_n T_n(\cos(\pi l/N)) \\ &= \sum_{n=0}^N a_n \cos(\pi n l/N) = \sum_{n=0}^N \frac{F_n}{c_n} \cos(\pi n l/N) \end{aligned}$$

This looks very much like a discrete cosine series and in fact one can show [4] that the coefficients  $F_n$  are related to the values  $f_l$  of the function by an inverse discrete Fourier transform (DCT)

$$F_n = \frac{2}{N} \sum_{l=0}^N \frac{f_l}{c_l} \cos(\pi n l/N).$$

Note, that up to a numerical factor the DCT is idempotent, i.e., it is its own inverse. This relationship between the Chebyshev polynomials and the DCT is the basis for the efficient computations because the DCT can be performed numerically by using the fast Fourier transform (FFT) and pre- and postprocessing of the coefficients [12]. The fast transform allows us to switch easily between the representations of the function in terms of its sampled values and in terms of the expansion coefficients  $a_n$  (or  $F_n$ ).

The fact that  $f$  is approximated globally by a finite sum of polynomials allows us to express any operation applied to  $f$  approximately in terms of the coefficients. Let us illustrate this in the case of integration. So we assume that  $f = p_N = \sum_{n=0}^N a_n T_n$  and we want to find an approximation of the integral for  $p_N$ , i.e., the function

$$F(x) = \int_{-1}^x f(s) ds,$$

so that  $F'(x) = f(x)$ . We make the ansatz  $F(x) = \sum_{n=0}^N b_n T_n(x)$  and obtain the equation

$$F' = \sum_{n=0}^N b_n T'_n = \sum_{n=0}^N a_n T_n = f.$$

Expressing  $T_n$  in terms of the  $T'_n$  using (17) and comparing coefficients implies the equations

$$b_1 = \frac{2a_0 - a_2}{2}, \quad b_n = \frac{a_{n-1} - a_{n+1}}{2n} \quad \text{for } 0 < n < N, \quad b_N = \frac{a_{N-1}}{2N}.$$

between the coefficients which determines all  $b_l$  in terms of the  $a_n$  except for  $b_0$ . This free constant is determined by the requirement that  $F(-1) = 0$  which implies (because  $T_n(-1) = (-1)^n$ )

$$b_0 = - \sum_{n=1}^N (-1)^n b_n.$$

These coefficients  $b_n$  determine a polynomial  $q_N$  of degree  $N$  which approximates the indefinite integral  $F(x)$  of the  $N$ -th degree polynomial  $f$ . The exact function is a polynomial of degree  $N+1$  whose highest coefficient is proportional to the highest coefficient  $a_N$  of  $f$ . Thus, ignoring this term we make an error whose magnitude is of the order of  $|a_N|$  so that the approximation will be the better the smaller  $|a_N|$  is. The same is true when a smooth function  $f$  is approximated by a polynomial  $p_N$ . Then, again, the indefinite integral will be approximated well by the polynomial  $q_N$  whose coefficients are determined as above provided the highest coefficients in the approximating polynomial  $p_N$  are small.

From the coefficients  $b_n$  we can also find an approximation to the definite integral  $\int_{-1}^1 f(s) ds = F(1)$  by evaluating

$$q_N(1) = \sum_{n=0}^N b_n = 2 \sum_{l=0}^{\lfloor N/2 \rfloor} b_{2l+1}.$$

Thus, to find an approximation of the integral of a function  $f$  we proceed as described above, first computing the coefficients  $a_n$  of  $f$ , computing the  $b_n$  and then calculating the sum of the odd coefficients.

**3.2. Implementation of the square-root.** The Riemann surface  $\mathcal{L}$  is defined by an algebraic curve of the form

$$\mu^2 = (K - \xi)(K - \bar{\xi}) \prod_{i=1}^g (K - E_i)(K - \bar{E}_i),$$

where in our case we have  $g = 2$  throughout. In order to compute the periods and the theta-functions related to this Riemann surface it is necessary to evaluate the square-root  $\sqrt{\mu^2(K)}$  for arbitrary complex numbers  $K$ . In order to make this a well defined problem we introduce the cut-system as indicated in Fig. 1. On the

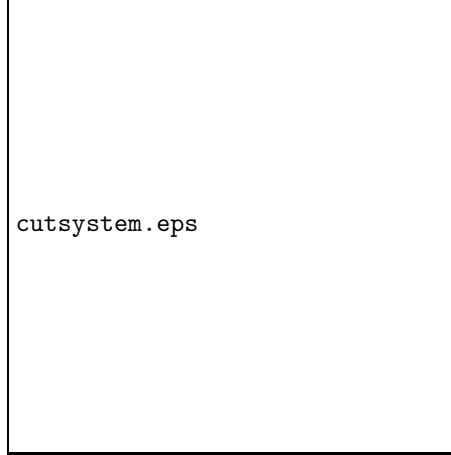


FIGURE 1. Canonical cycles ( $P_0 = \xi$ ).

cut surface the square-root  $\mu(K)$  is defined as in [17] as the product of square-roots of monomials

$$(19) \quad \mu = \sqrt{K - \xi} \sqrt{K - \bar{\xi}} \prod_{i=1}^g \sqrt{K - E_i} \sqrt{K - \bar{E}_i}.$$

The square-root routines such as the one available in MATLAB usually have their branch-cut along the negative real axis. The expression (19) is holomorphic on the cut surface so that we cannot simply take the builtin square-root when computing  $\sqrt{\mu^2(K)}$ . Instead we need to use the information provided by the cut-system to define adapted square-roots.

Let  $\arg(z)$  be the argument of a complex number  $z$  with values in  $] -\pi, \pi[$  and consider two factors in (19) such as

$$\sqrt{K - P_1} \sqrt{K - P_2}$$



where  $P_1$  and  $P_2$  are two branch-points connected by a branch-cut. Let  $\alpha = \arg(P_2 - P_1)$  be the argument at the line from  $P_1$  to  $P_2$ . Now we define the square-root  ${}^{(\alpha)}\sqrt{\cdot}$  with branch-cut along the ray with argument  $\alpha$  by computing for each  $z \in \mathbb{C}$  the square-root  $s := \sqrt{z}$  with the available MATLAB routine and then putting

$${}^{(\alpha)}\sqrt{z} = \begin{cases} s & \alpha/2 < \arg(s) < \alpha/2 + \pi \\ -s & \text{otherwise} \end{cases}.$$

With this square-root we compute the two factors

$${}^{(\alpha)}\sqrt{K - P_1} {}^{(\alpha)}\sqrt{K - P_2}.$$

It is easy to see that this expression changes sign exactly when the branch-cut between  $P_1$  and  $P_2$  is crossed. We compute the expression (19) by multiplying the pairs of factors which correspond to the branch-cuts.

This procedure is not possible in the case of the non-linear transformations we are using to evaluate the periods in certain limiting cases. In these cases the root is chosen in a way that the integrand is a continuous function on the path of integration.

**3.3. Numerical treatment of the periods.** The quantities entering formula (8) for the Ernst potential are the periods of the Riemann surface and the line integrals  $\mathbf{u}$  and  $I$ . The value of the theta-function is then approximated by a finite sum.

The periods of a hyperelliptic Riemann surface can be expressed as integrals between branch points. Since we need in our example the periods of the holomorphic differentials and the differential of the third kind with poles at  $\infty^\pm$ , we have to consider integrals of the form

$$(20) \quad \int_{P_i}^{P_j} \frac{K^n dK}{\mu(K)}, \quad n = 0, 1, 2,$$

where the  $P_i, i, j = 1, \dots, 6$  denote the branch points of  $\mathcal{L}$ .

In general position we use a linear transformation of the form  $K = ct + d$  to transform the integral (20) to the normal form

$$(21) \quad \int_{-1}^1 \frac{\alpha_0 + \alpha_1 t + \alpha_2 t^2}{\sqrt{1-t^2}} H(t) dt,$$

where the  $\alpha_i$  are complex constants and where  $H(t)$  is a continuous (in fact, analytic) complex valued function on the interval  $[-1, 1]$ . This form of the integral suggests to express the powers  $t^n$  in the numerator in terms of the first three Chebyshev polynomials  $T_0(t) = 1$ ,  $T_1(t) = t$  and  $T_2(t) = 2t^2 - 1$  and to approximate the function  $H(t)$  by a linear combination of Chebyshev polynomials

$$H(t) = \sum_{n \geq 0} h_n T_n(t).$$

The integral is then calculated with the help of the orthogonality relation (18) of the Chebyshev polynomials.

Since the Ernst potential has to be calculated for all  $\rho, \zeta \in \mathbb{R}_0^+$ , it is convenient to use the cut-system (1). In this system the moving cut does not cross the immovable cut. In addition the system is adapted to the symmetries and reality properties of  $\mathcal{L}$ . Thus the periods  $a_2$  and  $b_2$  are related to  $a_1$  and  $b_1$  via complex conjugation. For the analytical calculations of the Ernst potential in the limit of collapsing cuts, we have chosen in [21] cut systems adapted to the respective situation. In the limit  $\xi \rightarrow \bar{\xi}$  we were using for instance a system where  $a_2$  is the cycle around the cut  $[\xi, \bar{\xi}]$ . This has the effect that only the  $b$ -period  $b_2$  diverges logarithmically in this

case whereas the remaining periods stay finite as  $\rho$  tends to 0. In the cut systems 1, all periods diverge as  $\ln \rho$ . Since the divergence is only logarithmical this does not pose a problem for values of  $\rho > 10^{-5}$ . In addition the integrals which have to be calculated in the evaluation of the periods are the same in both cut-system. Thus there is no advantage in using different cut systems for the numerical work.

To test the numerics we use the fact that the integral of any holomorphic differential along a contour surrounding the cut  $[E_1, F_1]$  in positive direction is equal to minus the sum of all  $a$ -periods of this integral. Since this condition is not implemented in the code it provides a strong test for the numerics. It can be seen in Fig. 2 that 16 to 32 polynomials are sufficient in general position to achieve optimal accuracy. Since MATLAB works with 16 digits, machine precision is in general limited to 14 digits due to rounding errors. These rounding errors are also the reason why the accuracy drops slightly when a higher number of polynomials is used. The use of a low number of polynomials consequently does not only require less computational resources but has the additional benefit of reducing the rounding errors. It is therefore worthwhile to reformulate a problem if a high number of polynomials would be necessary to obtain optimal accuracy. These situations occur in the

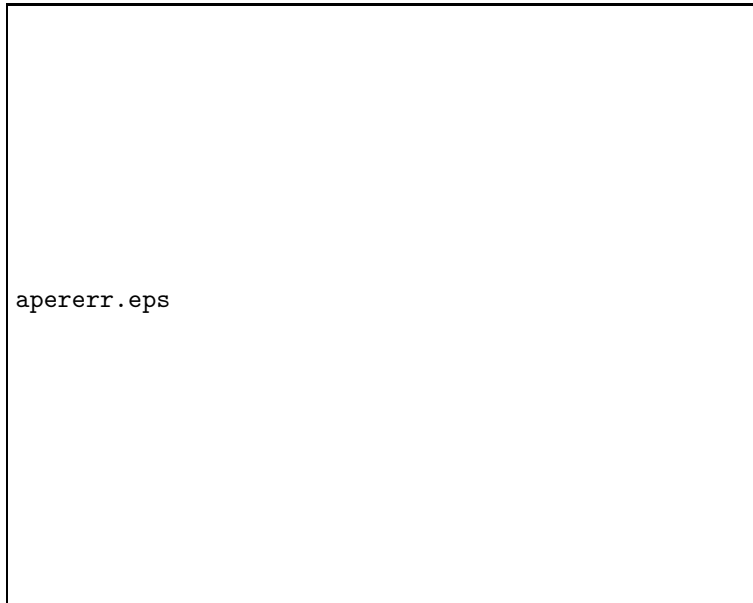


FIGURE 2. Test of the numerics for the  $a$ -periods at several points in the space-time. The error is shown in dependence of the number  $N$  of Chebyshev polynomials.

calculation of the periods when the moving branch points almost coincide which happens on the axis of symmetry in the space-time or at spatial infinity. As can be seen from Fig. 2, for  $\rho = 10^{-3}$  and  $\zeta = 10^3$  not even 2048 polynomials (this is the limit due to memory on the low end computers we were using) produce sufficient accuracy. The reason for these problems is that the function  $H$  in (21) behaves like  $1/\sqrt{t+\rho}$  near  $t = 0$ . For small  $\rho$  this behavior is only satisfactorily approximated by a large number of polynomials. We therefore split the integral in two integrals between  $F_2$  and  $(F_2 + \bar{\xi})/2$  and between  $(F_2 + \bar{\xi})/2$  and  $\bar{\xi}$ . The first integral is calculated with the Chebyshev integration routine after the substitution  $t = \sqrt{K - F_2}$ . This substitution leads to a regular integrand also at the branch point  $F_2$ . The second integral is calculated with the Chebyshev integration routine

after the substitution  $K - \zeta = \rho \sinh(t)$ . This takes care of the almost collapsing cut  $[\xi, \bar{\xi}]$ . It can be seen in Fig. 2 that 128 polynomials are sufficient to obtain machine precision even in almost degenerate situations.

The cut-system in Fig. 1 is adapted to the limit  $\bar{\xi} \rightarrow F_2$  in what concerns the  $a$ -periods, since the cut which collapses in this limit is encircled by an  $a$ -cycle. However there will be similar problems as above in the determination of the  $b$ -periods. For  $\bar{\xi} \sim F_2$  we split the integrals for the  $b$ -periods as above in two integrals between  $F_1$  and 0, and 0 and  $F_2$ . For the first integral we use the integration variable  $t = \sqrt{K - F_1}$ , for the second  $K = \Re F_2 - i\Im F_2 \sinh t$ . Since the Riemann matrix (the matrix of  $b$ -periods of the holomorphic differentials after normalization) is symmetric, the error in the numerical evaluation of the  $b$ -periods can be estimated via the asymmetry of the calculated Riemann matrix. We define the function  $err(\rho, \zeta)$  as the maximum of the norm of the difference in the  $a$ -periods discussed above and the difference of the off-diagonal elements of the Riemann matrix. This error is presented for a whole space-time in Fig. 3. The values for  $\rho$  and  $\zeta$  vary between  $10^{-4}$  and  $10^4$ . On the axis and at the disk we give the error for the elliptic integrals (only the error in the evaluation of the  $a$ -periods, since the Riemann matrix has just one component). For  $\xi \rightarrow \infty$  the asymptotic formulas for the Ernst potential are used. The calculation is performed with 128 polynomials, and up to 256 for  $|\xi| > 10^3$ . It can be seen that the error is in this case globally below  $10^{-13}$ .

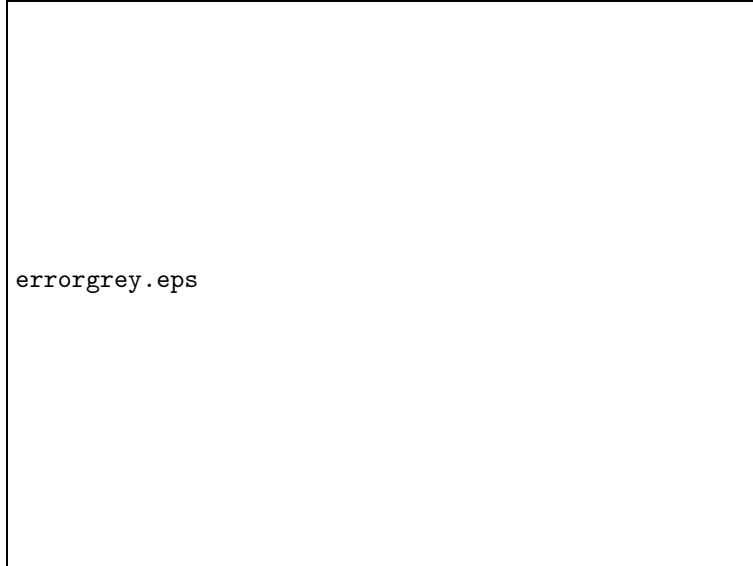


FIGURE 3. A measure for the error in the determination of the periods in dependence of the physical coordinates. For  $\rho, \zeta > 1$  we use  $1/\rho, 1/\zeta$  as coordinates.

**3.4. Numerical treatment of the line integrals.** The line integrals  $\mathbf{u}$  and  $I$  in (8) are linear combinations of integrals of the form

$$(22) \quad \int_{-i}^i \frac{\ln G(K) K^l dK}{\mu(K)}, \quad l = 0, 1, 2.$$

In general position, i.e. not close to the disk and  $\lambda$  small enough, the integrals can be directly calculated after the transformation  $K = it$  with the Chebyshev

integration routine. To test the numerics we consider the Newtonian limit ( $\lambda \rightarrow 0$ ) where the function  $\ln G$  is proportional to  $1 + K^2$ , i.e. we calculate the test integral

$$(23) \quad \int_{-i}^i \frac{(1 + K^2) dK}{\sqrt{(K - \zeta)^2 + \rho^2}}.$$

We compare the numerical with the analytical result in Fig. 4. In general position machine precision is reached with 32 polynomials.

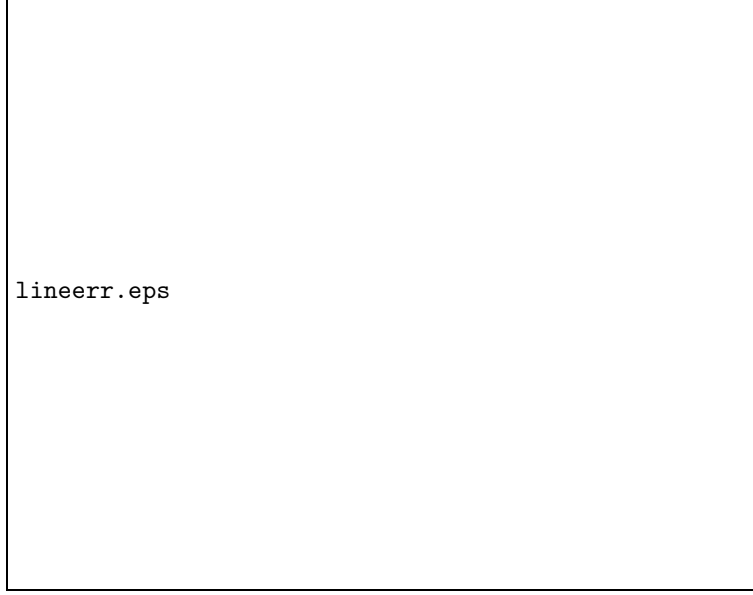


FIGURE 4. Error in the integrals for the Maclaurin solution in dependence of the number  $N$  of Chebyshev polynomials.

When the moving cut approaches the path  $\Gamma$ , i.e., when the space-time point comes close to the disk, the integrand in (23) develops cusps near the points  $\xi$  and  $\bar{\xi}$ . In this case a satisfactory approximation becomes difficult even with a large number of polynomials. Therefore we split the integration path in  $[-i, -i\rho]$ ,  $[-i\rho, i\rho]$  and  $[i\rho, i]$ . Using the reality properties of the integrands, we only calculate the integrals between 0 and  $i\rho$ , and between  $i\rho$  and  $i$ . In the first case we use the transformation  $K = \zeta + \rho \sinh t$  to evaluate the integral with the Chebyshev integration routine, in the second case we use the transformation  $t = \sqrt{K - \xi}$ . It can be seen in figure 4 that machine precision can be reached even at the disk with 64 to 128 polynomials. The values at the disk are, however, determined in terms of elliptic functions which is more efficient than the hyperelliptic formulae.

To treat the case where  $\delta\lambda^2$  is not small, it is convenient to rewrite the function  $G$  in (11) in the form

$$(24) \quad \ln G(K) = 2 \ln \left( \sqrt{(K^2 - \alpha)^2 + \beta^2} + K^2 + 1 \right) - \ln \left( \frac{1}{\lambda^2} - \delta K^2 \right).$$

In the limit  $\delta\lambda^2 \rightarrow \infty$  with  $\delta$  finite, the second term in (24) becomes singular for  $K = 0$ . Even for  $\delta\lambda^2$  large but finite, the approximation of the integrand by Chebyshev polynomials requires a huge number of coefficients as can be seen from Fig. 5. It is therefore sensible to ‘regularize’ the integrand near  $K = 0$ . We consider

instead of the function  $\ln(\frac{1}{\lambda^2} - \delta K^2)F(K)$  where  $F(K)$  is a  $C^\infty$  function near  $K = 0$ , the function

$$(25) \quad \ln\left(\frac{1}{\lambda^2} - \delta K^2\right) \left( F(K) - F(0) - F'(0)K - \dots - \frac{1}{n!}F^{(n)}(0)K^n \right).$$

The parameter  $n$  is chosen such that the spectral coefficients of (25) are of the order of  $10^{-14}$  for a given number of polynomials, see Fig. 5. There we consider the integral

$$(26) \quad \int_{-i}^i \frac{\ln G(K) dK}{\sqrt{(K^2 - \alpha)^2 + \beta^2}},$$

which has to be calculated on the axis. We show the absolute values of the coefficients  $a_k$  in an expansion of the integrand in Chebyshev polynomials,  $\sum_{k=1}^N a_k T_k$ . It can be seen that one has to include values of  $n = 6$  in (25). The integral  $\int_\Gamma \ln G(K)F(K)$  is then calculated numerically as the integral of the function (25), the subtracted terms are integrated analytically. In this way one can ensure that



FIGURE 5. Spectral coefficients for the integral (26) for  $\delta = 1$  and  $\lambda = 10^{16}$  in dependence of the number of Chebyshev polynomials.

the line integrals are calculated in the whole space-time with machine precision: close to the Newtonian limit, we use an analytically known test function to check the integration routine, for general situations we check the quality of the approximation of the integrand by Chebyshev polynomials via the spectral coefficients which have to become smaller than  $10^{-14}$ .

**3.5. Theta-functions.** The theta series (5) for the Riemann theta-function (the theta function in (5) with zero characteristic, theta functions with characteristic follow from (6)) is approximated as the sum

$$(27) \quad \Theta(\mathbf{x}|\mathbf{B}) = \sum_{n_1=-N}^N \sum_{n_2=-N}^N \exp \left\{ \frac{1}{2} n_1^2 B_{11} + n_1 n_2 B_{12} + \frac{1}{2} B_{22} + n_1 x_1 + n_2 x_2 \right\}.$$

The value of  $N$  is determined by the condition that terms in the series (5) for  $n > N$  are strictly smaller than some threshold value  $\epsilon$  which is taken to be of the order of  $10^{-16}$ . To this end we determine the eigenvalues of  $\mathbf{B}$  and demand that

$$(28) \quad N > -\frac{1}{B_{max}} \left( \|\mathbf{x}\| + \sqrt{\|\mathbf{x}\|^2 + 2 \ln \epsilon B_{max}} \right),$$

where  $B_{max}$  is the real part of the eigenvalue with maximal real part ( $\mathbf{B}$  is negative definite). For a more sophisticated analysis of theta summations see [6]. In general position we find values of  $N$  between 4 and 8. For very large values of  $\zeta$  close to the axis,  $N$  can become larger than 40 which however did not lead to any computational problems. To treat more extreme cases it could be helpful to take care of the fact that the eigenvalues of  $\mathbf{B}$  can differ by more than an order of magnitude in our example. In these cases a summation over an ellipse rather than over a sphere in the plane  $(n_1, n_2)$ , i.e. different limiting values for  $n_1$  and  $n_2$  as in [6] will be more efficient.

In our case the computation of the integrals entering the theta-functions was however always the most time consuming such that an optimization of the summation of the theta-function would not have a noticeable effect. Due to the vectorization techniques in MATLAB, the theta summation always took less than 10 % of the calculation time for a value of the Ernst potential. Between 50 and 70 % of the processor time are used for the determination of the periods. On the used low-end PCs, the calculation time varied between 0.4 and 1.2s depending on the used number of polynomials. We show a plot of the real part of the Ernst potential for  $\lambda = 10$  and  $\delta = 1$  in Fig. 6. For  $\rho, \zeta > 1$ , we use  $1/\rho, 1/\zeta$  as coordinates which makes it possible to plot the whole space-time in Weyl coordinates. The non-smoothness of the coordinates across  $\rho = 1 = 1/\rho$  and  $\zeta = 1 = 1/\zeta$  is noticeable in the plot. Asymptotically the potential is equal to 1. The disk is situated in the equatorial plane between  $\rho = 0$  and  $\rho = 1$ . At the disk, the normal derivatives of  $f$  are discontinuous.

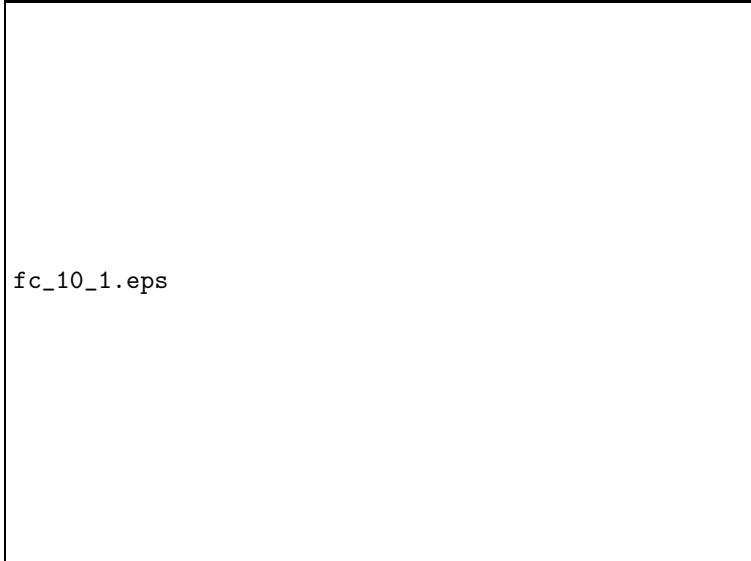


FIGURE 6. The real part of the Ernst potential for  $\lambda = 10$  and  $\delta = 1$  in dependence of the physical coordinates. For  $\rho, \zeta > 1$  we use  $1/\rho, 1/\zeta$  as coordinates.

The imaginary part of the Ernst potential in this case is given in Fig. 7. It vanishes at infinity and at the regular part of the equatorial plane. At the disk, the potential has a jump.

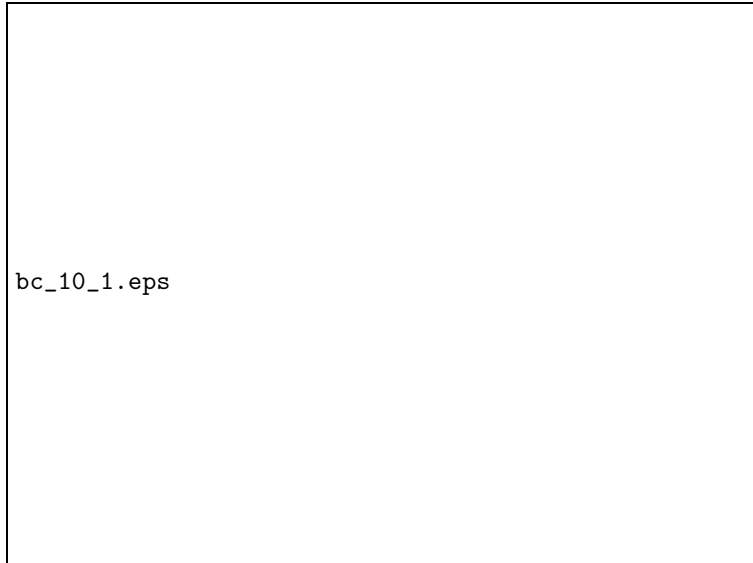


FIGURE 7. The imaginary part of the Ernst potential for  $\lambda = 10$  and  $\delta = 1$  in dependence of the physical coordinates. For  $\rho, \zeta > 1$  we use  $1/\rho, 1/\zeta$  as coordinates.

#### 4. INTEGRAL IDENTITIES

In the previous section we have tested the accuracy of the numerics locally, i.e. at single points in the space-time. Integral identities have the advantage that they provide some sort of global test of the numerical precision since they sum up the errors. In addition they require the calculation of the potentials in extended regions of the space-time which allows to explore the numerics for rather general values of the physical coordinates.

The identities we are considering in the following are the well known equivalence of a mass calculated at the disk (the Komar mass) and the ADM mass determined at infinity, see [24, 34], and a generalization of the Newtonian virial identity, see [15] and the appendix. The derivatives of the Ernst potential occurring in the integrands can be related to derivatives of theta-functions, see [21]. Since we are interested here in the numerical treatment of theta-functions with spectral methods, we determine the derivatives with spectral methods, too (see section 3). The integrals are again calculated with the Chebyshev integration routine. The main problem in this context is the singular behavior of the integrands e.g. at the disk which is a singularity for the space-time. As before this will lead to problems in the approximation of these terms via Chebyshev polynomials. This could lead to a drop in accuracy which is mainly due to numerical errors in the evaluation of the integrand and not of the potentials which we want to test. An important point is therefore the use of integration variables which are adapted to the possible singularities.

**4.1. Mass equalities.** The equality between the ADM mass and the Komar mass provides a test of the numerical treatment of the elliptic theta-functions at the

disk by means of the elliptic theta-functions on the axis. Since this equality is not implemented in the code, it provides a strong test.

The Komar mass at the disk is given by formula (42) of the appendix. In the example we are considering here, the normal derivatives at the disk can be expressed via tangential derivatives (see [13]) which makes a calculation of the derivatives solely within the disk possible. We implement the Komar mass in the form

$$(29) \quad m_K = \int_0^1 d\rho \frac{b_\rho}{4\Omega^2 \sqrt{\rho^2 - \delta f^2 + 2f/\lambda}} \left( f + \frac{\Omega^2}{f} (\rho^2 - a^2 f^2) \right).$$

The integrand is known to vanish as  $\sqrt{1 - \rho^2}$  at the rim of the disk, which is the typical behavior for such disk solutions. Since  $\sqrt{1 - \rho^2}$  is not analytic in  $\rho$ , an expansion of the integrand (29) in Chebyshev polynomials in  $\rho$  would not be efficient. We will thus use  $t = \sqrt{1 - \rho^2}$  as the integration variable. This takes care of the behavior at the rim of the disk. Since in general the integrand in 29 depends on  $\rho^2$ , this variable can be used in the whole disk. In the ultra-relativistic limit for  $\delta \neq 0$ , the function  $f$  vanishes as  $\rho$ . In such cases it is convenient either to take two domains of integration or to use a different variable of integration. We chose the second approach with  $\rho = \sin x$  (this corresponds to the disk coordinates (30)). Yet, strongly relativistic situations still lead to problems since  $f$  vanishes in this case at the center of the disk as does  $b_\rho$  which leads to a ‘0/0’ limit. In Fig. 8 one can see that the masses are in general equal to the order of  $10^{-14}$ . In these calculations 128 up to 256 polynomials were used. We show the dependence for  $\gamma = 0.7$  and several values of  $\epsilon$ , as well as for  $\epsilon = 0.8$  and several values of  $\gamma$ . The accuracy drops in the strongly relativistic, almost static situations ( $\epsilon$  close to 1,  $\gamma$  close to zero) since the Riemann surface is almost degenerate in this case ( $\beta \rightarrow 0$ ). In the ultra-relativistic limit for  $\delta = 0$ , the situation is no longer asymptotically flat which implies that the masses formally diverge. For  $\epsilon = 0.95$ , the masses are still equal to the order of  $10^{-13}$ . Not surprisingly the accuracy drops for  $\epsilon = 0.9996$  to the order of  $10^{-4}$ .

**4.2. Virial-type identities.** Generalizations of the Newtonian virial theorem are used in numerics (see [15]) as a test of the quality of the numerical solution of the Einstein equations. Since they involve integrals over the whole space-time, they test the numerics globally and thus provide a valid criterion for the entire range of the physical coordinates.

The identity which is checked here is a variant of the one given in [15] which is adapted to possible problems at the zeros of the real part of the Ernst potential, the so-called ergosphere, see [13] for the disk solutions discussed here. Eq. (45) relates integrals of the Ernst potential and its derivatives over the whole space-time to corresponding integrals at the disk. Since the numerics at the disk has been tested above, this provides a global test of the evaluation of the Ernst potential. As before, derivatives and integrals will be calculated via spectral methods.

The problem one faces when integrating over the whole space-time is the singular behavior of the fields on the disk which represents a discontinuity of the Ernst potential. The Weyl coordinates in which the solution is given are not optimal to describe the geometry near the disk. Hence a huge number of polynomials is necessary to approximate the integrands in (45). Even with 512 polynomials for each coordinate, the coefficients of an expansion in Chebyshev polynomials did not drop below  $10^{-6}$  in more relativistic situations. Though the computational limits are reached, the identity (45) is only satisfied to the order of  $10^{-8}$  which is clearly related to the bad choice of coordinates.



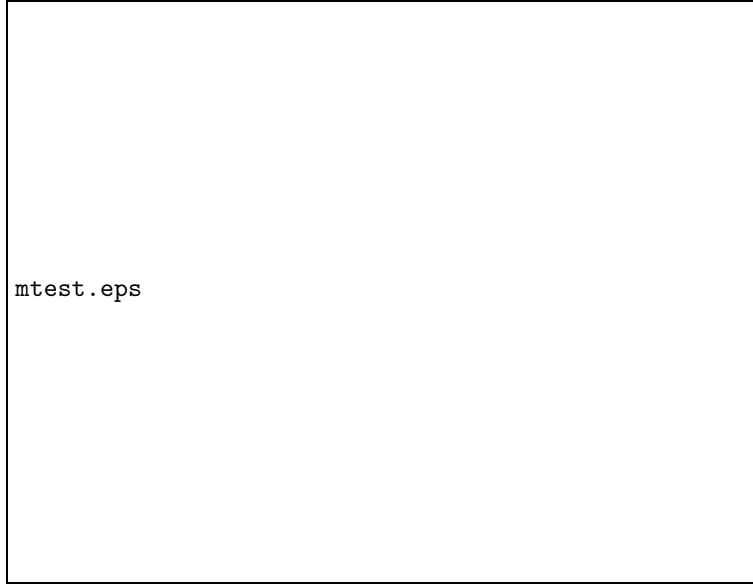


FIGURE 8. The relative difference of the ADM mass and the Komar mass for  $\gamma = 0.7$  and several values of  $\epsilon$ , and for  $\epsilon = 0.8$  and several values of  $\gamma$ .

We therefore use for this calculation so-called disk coordinates  $\eta, \theta$  (see [3]) which are related to the Weyl coordinates via

$$(30) \quad \rho + i\zeta = \cosh(\eta + i\theta).$$

The coordinate  $\eta$  varies between  $\eta = 0$ , the disk, and infinity, the coordinate  $\theta$  between  $-\pi/2$  and  $\pi/2$ . The axis is given by  $\pm\pi/2$ , the equatorial plane in the exterior of the disk by  $\theta = 0$  and  $\eta \neq 0$ . Because of the equatorial symmetry, we consider only positive values of  $\theta$ . The surfaces of constant  $\eta$  are confocal ellipsoids which approach the disk for small  $\eta$ . For large  $\eta$ , the coordinates are close to spherical coordinates.

To evaluate the integrals in (45), we perform the  $\eta$ -integration up to a value  $\eta_0$  as well as the  $\theta$ -integration with the Chebyshev integration routine. The parameter  $\eta_0$  is chosen in a way that the deviation from spherical coordinates becomes negligible, typically  $\eta_0 = 15$ . The integral from  $\eta_0$  to infinity is then carried out analytically with the asymptotic formula (14). It turns out that an expansion in 64 to 128 polynomials for each coordinate is sufficient to provide a numerically optimal approximation within the used precision. This illustrates the convenience of the disk coordinates in this context. The virial identity is then satisfied to the order of  $10^{-12}$ . We plot the deviation of the sum of the integrals in (45) from zero for several values of  $\lambda$  and  $\gamma$  in Fig. 9. The drop in accuracy for strongly relativistic almost static situations ( $\gamma$  small and  $\epsilon$  close to 1) is again due to the almost degenerate Riemann surface. The lower accuracy in the case of strongly relativistic situations for  $\gamma = 1$  reflects the fact that the disk is shrinking to a point in this limit. To maintain the needed resolution one would have to use more polynomials in the evaluation of the virial-type identity which was not possible on the used computers.

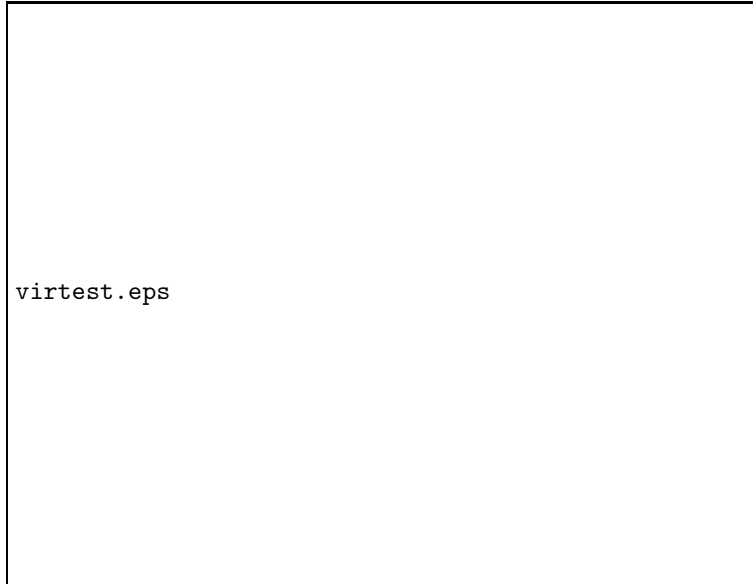


FIGURE 9. The deviation from zero of the virial-type identity for  $\gamma = 0.7$  and several values of  $\epsilon$ , and for  $\epsilon = 0.8$  and several values of  $\gamma$ .

## 5. TESTING LORENE

One purpose of exact solutions of the Einstein equations is to provide test-beds for numerical codes to check the quality of the numerical approximation. In the previous sections we have established that the theta-functional solutions can be numerically evaluated to the order of machine precision which implies they can be used in this respect.

The code we are considering here is a C++-library called LORENE [35] which was constructed to treat problems from relativistic astrophysics such as rapidly rotating neutron stars. The main idea is to solve Poisson-type equations iteratively via spectral methods. To this end an equation as the Ernst equation (1) is written in the form

$$(31) \quad \Delta \mathcal{F} = \mathcal{G}(\mathcal{F}, r, \theta, \phi),$$

where spherical coordinates  $r, \theta, \phi$  are used, and where  $\mathcal{G}$  is some possibly non-linear functional of  $\mathcal{F}$  and the coordinates. The system (31) is to be solved for  $\mathcal{F}$  which can be a vector. In an iterative approach, the equation is rewritten as

$$(32) \quad \Delta \mathcal{F}_{n+1} = \mathcal{G}(\mathcal{F}_n, r, \theta, \phi), \quad n = 1, 2, \dots$$

Starting from some initial function  $\mathcal{F}_0$ , in each step of the iteration a Poisson equation is solved for a known right-hand side. For the stationary axisymmetric Einstein equations which we are considering here, it was shown in [31] that this iteration will converge exponentially for small enough boundary data if the initial values are close to the solution of the equation in some Banach space norm. It turns out that one can always start the iteration with Minkowski data, but it is necessary to use a relaxation: instead of the solution  $\mathcal{F}_{n+1}$  of (32), it is better to take a combination  $\tilde{\mathcal{F}}_{n+1} = \mathcal{F}_{n+1} + \kappa \mathcal{F}_n$  with  $\kappa \in ]0, 1[$  (typically  $\kappa = 0.5$ ) as a new value in the source  $\mathcal{G}_{n+1}$  to provide numerical stability. The iteration is in general stopped if  $\|\mathcal{F}_{n+1} - \mathcal{F}_n\| < 10^{-10}$ .

The Ernst equation (1) is already in the form (31), but it has the disadvantage that the equation is no longer strongly elliptic at the ergo-sphere where  $\Re(\mathcal{E}) = 0$ . In physical terms, this apparent singularity is just a coordinate singularity, and the theta-functional solutions are analytic there. The Ernst equation in the form (31) has a right-hand side of the form ‘0/0’ for  $\Re\mathcal{E} = 0$  which causes numerical problems especially in the iteration process since the zeros of the numerator and the denominator will only coincide for the exact solution. The disk solutions we are studying here have ergo-spheres in the shape of cusped toroids (see [13]). Therefore it is difficult to take care of the limit 0/0 by using adapted coordinates. Consequently the use of the Ernst picture is restricted to weakly relativistic situations without ergo-spheres in this framework.

To be able to treat strongly relativistic situations, we use a different form of the stationary axisymmetric vacuum Einstein equations which is derived from the standard 3 + 1-decomposition, see [16]. We introduce the functions  $\nu$  and  $N_\phi$  via

$$(33) \quad e^{2\nu} = \frac{\rho^2 f}{\rho^2 - a^2 f^2}, \quad N_\phi = \frac{\rho a f^2}{\rho^2 - a^2 f^2},$$

where  $ae^{2U}$  is the  $g_{t\phi}$  component of the metric leading to the Ernst potential, see (37) in the appendix. Expressions for  $a$  in terms of theta-functions are given in [13]. The vacuum Einstein equations for the functions (33) read

$$(34) \quad \Delta\nu = \frac{1}{2}\rho^2 e^{-4\nu} (N_{\phi,\rho}^2 + N_{\phi,\zeta}^2),$$

$$(35) \quad \Delta N_\phi - \frac{1}{\rho^2} N_\phi = 4\rho (N_{\phi,\rho}(e^{2\nu})_\rho + N_{\phi,\zeta}(e^{2\nu})_\zeta).$$

By putting  $V = N_\phi \cos\phi$  we obtain the flat 3-dimensional Laplacian acting on  $V$  on the left-hand side,

$$(36) \quad \Delta V = 4\rho (V_\rho(e^{2\nu})_\rho + V_\zeta(e^{2\nu})_\zeta).$$

Since the function  $e^{2\nu}$  can only vanish at a horizon, it is globally non-zero in the examples we are considering here. Thus the system of equations (34) and (36) is strongly elliptic, even at an ergo-sphere.

The disadvantage of this regular system is the non-linear dependence of the potentials  $\nu$  and  $N_\phi$  on the Ernst potential and  $a$  via (33). Thus we loose accuracy due to rounding errors of roughly an order of magnitude. Though we have shown in the previous sections that we can guarantee the numerical accuracy of the data for  $f$  and  $af$  to the order of  $10^{-14}$ , the values for  $\nu$  and  $V$  are only reliable to the order of  $10^{-13}$ .

To test the spectral methods implemented in **LORENE**, we provide boundary data for the disk solutions discussed above on a sphere around the disk. For these solutions it would have been more appropriate to prescribe data at the disk, but **LORENE** was developed to treat objects of spherical topology such as stars which suggests the use of spherical coordinates. It would be possible to include coordinates like the disk coordinates of the previous section in **LORENE**, but this is beyond the scope of this article. Instead we want to use the Poisson-Dirichlet routine which solves a Dirichlet boundary value problem for the Poisson equation for data prescribed at a sphere. We prescribe the data for  $\nu$  and  $N_\phi$  on a sphere of radius  $R$  and solve the system (34) and (36) iteratively in the exterior of the sphere. If the iteration converges, we compare the numerical solution in the exterior of the sphere with the exact solution.

Since spherical coordinates are not adapted to the disk geometry, a huge number of spherical harmonics would be necessary to approximate the potentials if  $R$  is close

to the disk radius. The limited memory on the used computers imposes an upper limit of 64 to 128 harmonics. We choose the radius  $R$  and the number of harmonics in a way that the Fourier coefficients in  $\theta$  drop below  $10^{-14}$  to make sure that the provided boundary data contain the related information to the order of machine precision. The exterior of the sphere where the boundary data are prescribed is divided in two domains, one from  $R$  to  $2R$  and one from  $2R$  to infinity. In the second domain  $1/r$  is used as a coordinate. For the  $\phi$  dependence which is needed only for the operator in (36), 4 harmonics in  $\phi$  are sufficient.

Since LORENE is adapted to the solution of the Poisson equation, it is to be expected that it reproduces the exact solution best for nearly static situations, since the static solutions solve the Laplace equation. The most significant deviations from the exact solution are therefore expected for  $\delta = 0$ . For the case  $\lambda = 3$ , we consider 32 harmonics in  $\theta$  on a sphere of radius  $R = 1.5$ . The iteration is stopped if  $||\mathcal{F}_{n+1} - \mathcal{F}_n| < 5 * 10^{-10}$  which is the case in this example after 90 steps. The exact solution is reproduced to the order of  $10^{-11}$ . The absolute value of the difference between the exact and the numerical solution on a sphere of radius 3 is plotted in Fig. 10 in dependence of  $\theta$ . There is no significant dependence of the error on  $\theta$ . The maximal deviation is typically found on or near the axis. As can be seen from



FIGURE 10. Difference between the exact and the numerical solution for  $\lambda = 3$  and  $\delta = 0$  for  $r = 3$  in dependence on  $\theta$ .

Fig. 11 which gives the dependence on  $r$  on the axis, the error decreases almost linearly with  $1/r$  except for some small oscillations near infinity.

We have plotted the maximal difference between the numerical and the exact solution for a range of the physical parameters  $\lambda$  and  $\delta$  in Fig. 12. As can be seen, the expectation is met that the deviation from the exact solution increases if the solution becomes more relativistic (larger  $\epsilon$ ). As already mentioned, the solution can be considered as exactly reproduced if the deviation is below  $10^{-13}$ . Increasing the value of  $\gamma$  for fixed  $\epsilon$  leads to less significant effects though the solutions become less static with increasing  $\gamma$ .

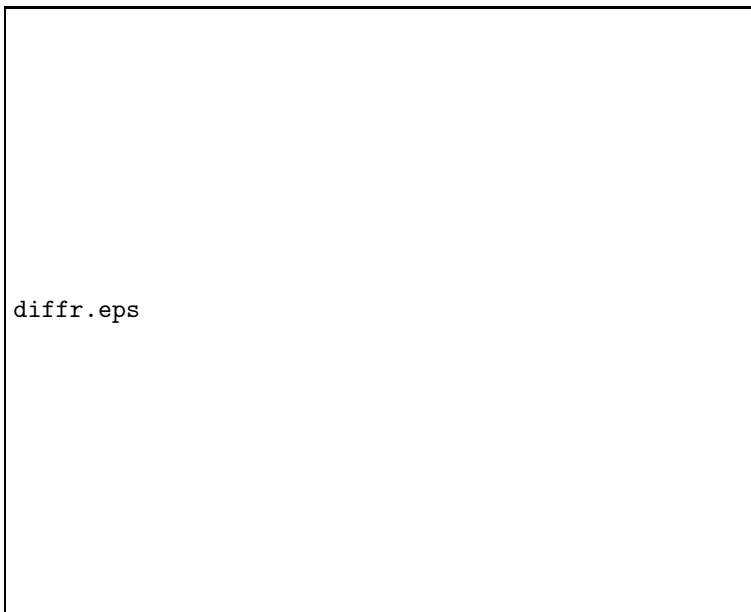


FIGURE 11. Difference between the exact and the numerical solution for  $\lambda = 3$  and  $\delta = 0$  on the axis in dependence on  $r$ .



FIGURE 12. Difference between the exact and the numerical solution for  $\gamma = 0.7$  and several values of  $\epsilon$ , and for  $\epsilon = 0.8$  and several values of  $\gamma$ .

,

For  $\delta = 0$ , the ultra-relativistic limit  $\lambda \rightarrow 4.629 \dots$  corresponds to a space-time with a singular axis which is not asymptotically flat, see [13]. Since **LORENE** expands all functions in a Galerkin basis with regular axis in an asymptotically flat setting, solutions close to this singular limit cannot be approximated. Convergence gets much slower and can only be achieved with considerable relaxation. For  $\lambda = 4$  and

$\delta = 0$  we needed nearly 2000 iterations with a relaxation parameter of  $\kappa = 0.9$ . The approximation is rather crude (in the order of one percent). For higher values of  $\lambda$  no convergence could be obtained.

This is however due to the singular behavior of the solution in the ultra-relativistic limit. In all other cases, **LORENE** is able to reproduce the solution to the order of  $10^{-11}$  and better, more static and less relativistic cases are reproduced with the provided accuracy.

## 6. CONCLUSION

In this article we have presented a scheme based on spectral methods to treat hyperelliptic theta-functions numerically. It was shown that an accuracy of the order of machine precision could be obtained with an efficient code. As shown, spectral methods are very convenient if analytic functions are approximated. Close to singularities such as the degeneration of the Riemann surface, analytic techniques must be used to end up with analytic integrands in the discussed example.

The obtained numerical data were used to provide boundary values for the code **LORENE** which made possible a comparison of the numerical solution to the boundary value problem with the numerically evaluated theta-functions. For a large range of the physical parameters the numerical solution was of the same quality as the provided data. The main errors in **LORENE** are introduced by rounding errors in the iteration. This shows that spectral methods provide a reliable and efficient numerical treatment both for elliptic equations and for hyperelliptic Riemann surfaces. However, to maintain the global quality of the numerical approximation an analytical understanding of the solutions is necessary in order to treat the non-analyticities of the solutions.

## APPENDIX A. EINSTEIN EQUATIONS AND INTEGRAL IDENTITIES

The Ernst equation has a geometric interpretation in terms of the stationary axisymmetric Einstein equations in vacuum. The metric can be written in this case in the Weyl-Lewis-Papapetrou form (see [27])

$$(37) \quad ds^2 = g_{ab}dx^a dx^b = -f(dt + ad\phi)^2 + (e^{2k}(d\rho^2 + d\zeta^2) + \rho^2 d\phi^2)/f,$$

where  $\rho$  and  $\zeta$  are Weyl's canonical coordinates and  $\partial_t$  and  $\partial_\phi$  are the commuting asymptotically timelike respectively spacelike Killing vectors.

In this case the vacuum field equations are equivalent to the Ernst equation (1) for the complex potential  $\mathcal{E}$ . For a given Ernst potential, the metric (37) can be constructed as follows: the metric function  $f$  is equal to the real part of the Ernst potential. The functions  $a$  and  $k$  can be obtained via a line integration from the equations

$$(38) \quad a_\xi = 2\rho \frac{(\mathcal{E} - \bar{\mathcal{E}})_\xi}{(\mathcal{E} + \bar{\mathcal{E}})^2},$$

and

$$(39) \quad k_\xi = (\xi - \bar{\xi}) \frac{\mathcal{E}_\xi \bar{\mathcal{E}}_\xi}{(\mathcal{E} + \bar{\mathcal{E}})^2}.$$

This implies that  $a$  is the dual of the imaginary part of the Ernst potential. The equation (39) for  $k$  follows from the equations

$$(40) \quad R_{\alpha\beta} = \frac{1}{2f^2} \Re(\mathcal{E}_\alpha \bar{\mathcal{E}}_\beta), \quad \alpha, \beta = 1, 2, 3,$$

where  $R$  is the (three-dimensional) Ricci tensor corresponding to the spatial metric  $h = \text{diag}(e^{2k}, e^{2k}, \rho^2)$ . This reflects a general structure of the vacuum Einstein equations in the presence of a Killing vector. For the Ricci scalar one finds

$$(41) \quad -\frac{1}{2}e^{2k}R = k_{\rho\rho} + k_{\zeta\zeta}.$$

We denote by  $h$  the determinant of the metric  $h$ .

The Komar integral [24, 34] of the twist of the timelike Killing vector  $\xi = \partial_t$  over the whole spacetime establishes the equivalence between the asymptotically defined ADM mass and the Komar mass  $m_K$ ,

$$(42) \quad 2 \int_{disk} dV \left( T_{ab} - \frac{1}{2}g_{ab}T_c^c \right) n^a \xi^b =: m_K,$$

where the integration is carried out over the disk, where  $n_a$  is the normal at the disk, and where  $T_{ab}$  is the energy momentum tensor of the disk given in [13]. In other words the ADM mass can be calculated either asymptotically or locally at the disk.

To obtain an identity which does not involve only surface integrals, we consider as in [15] an integral over the trace of equation (40) for the Ricci-tensor,

$$(43) \quad R = \frac{h^{\alpha\beta} \mathcal{E}_\alpha \bar{\mathcal{E}}_\beta}{2f^2}.$$

To avoid numerical problems at the set of zeros of  $f$ , the so-called ergo-sphere (see [13] for the disk solutions studied here), we multiply both sides of equation (40) by  $f^3$ . Integrating the resulting relation over the whole space-time, we find after partial integration

$$(44) \quad - \int_0^1 d\rho \rho f^3 k_\zeta + \int_0^\infty d\rho \int_{-\infty}^\infty d\zeta ((\rho f^3)_\rho k_\rho + (\rho f^3)_\zeta k_\zeta) = \int_0^\infty d\rho \int_{-\infty}^\infty d\zeta \rho f (\mathcal{E}_\rho \bar{\mathcal{E}}_\rho + \mathcal{E}_\zeta \bar{\mathcal{E}}_\zeta);$$

here the only contributions of a surface integral arise at the disk, since  $k \propto 1/r^2$  for  $r \rightarrow \infty$  and since the axis is regular ( $k$  vanishes on the axis). If we replace  $k$  via (39), we end up with an identity for the Ernst potential and its derivatives,

$$(45) \quad - \int_0^1 d\rho \rho^2 f (\mathcal{E}_\rho \bar{\mathcal{E}}_\zeta + \mathcal{E}_\zeta \bar{\mathcal{E}}_\rho) + \frac{3}{2} \int_0^\infty \int_0^\infty d\rho d\zeta \rho^2 (\mathcal{E}_\rho (\bar{\mathcal{E}}_\rho^2 + \bar{\mathcal{E}}_\zeta^2) + \bar{\mathcal{E}}_\rho (\mathcal{E}_\rho^2 + \mathcal{E}_\zeta^2)) \\ = 2 \int_0^\infty \int_0^\infty d\rho d\zeta \rho f \mathcal{E}_\zeta \bar{\mathcal{E}}_\zeta.$$

This identity (as the identity given in [15]) can be seen as a generalization of the Newtonian virial theorem. The relation (45) coincides with the corresponding relation of [15] only in the Newtonian limit. This reflects the fact that generalizations of a Newtonian result to a general relativistic setting are not unique. Our formulation is adapted to the Ernst picture and avoids problems at the ergo-spheres, thus it seems optimal to test the numerics for Ernst potentials in terms of theta-functions.

#### ACKNOWLEDGMENT

We thank A. Bobenko, D. Korotkin, E. Gourgoulhon and J. Novak for helpful discussions and hints. CK is grateful for financial support by the Marie-Curie program of the European Union and the Schloessmann foundation.

## REFERENCES

- [1] V.A. Belinskii, V.E. Zakharov, Integration of the Einstein equations by the methods of inverse scattering theory and construction of explicit multisoliton solutions, *Sov. Phys. JETP* **48** (1978) 985-994.
- [2] E. D. Belokolos, A. I. Bobenko, V. Z. Enolskii, A. R. Its and V. B. Matveev, *Algebro-Geometric Approach to Nonlinear Integrable Equations*, Berlin: Springer, (1994).
- [3] J. Binney and S. Tremaine, *Galactic Dynamics* (Princeton Univ. Press, Princeton, 1987).
- [4] W. L. Briggs and V. E. Henson, *The DFT, an owner's manual for the discrete Fourier transform*, Siam Philadelphia, 1995.
- [5] B. Deconinck and M. van Hoeij, Computing Riemann matrices of algebraic curves, *Physica D*, **152-153**, 28 (2001).
- [6] B. Deconinck, M. Heil, A. Bobenko, M. van Hoeij and M. Schmies, Computing Riemann Theta Functions, to appear in *Mathematics of Computation*.
- [7] B.A. Dubrovin, V.B. Matveev, S.P. Novikov, Non-linear equations of Korteweg-de Vries type, finite-zone linear operators, and Abelian varieties, *Russian Math. Surveys*, **31** 59-146 (1976)
- [8] B.A. Dubrovin, Theta functions and non-linear equations, *Russ. Math. Surv.* **36**, 11 (1981).
- [9] V.Z. Enolski, P.H. Richter, Periods of hyperelliptic integrals expressed in terms of  $\theta$ -constants by means of Thomae formulae, to appear in *Phil. Trans. London Math. Soc.*, (2003).
- [10] F.J. Ernst, New formulation of the axially symmetric gravitational field problem, *Phys. Rev.* **167**, 1175 (1968).
- [11] J.D. Fay, *Theta-functions on Riemann surfaces*, Lect. Notes in Math. **352**, Springer (1973)
- [12] B. Fornberg, *A practical guide to pseudospectral methods*, Cambridge University Press, Cambridge (1996)
- [13] J. Frauendiener and C. Klein, Exact relativistic treatment of stationary counter-rotating dust disks: physical properties, *Phys. Rev. D* **63**, 84025 (2001).
- [14] P. Gianni, M. Seppälä, R. Silhol, B. Trager, Riemann Surfaces, Plane Algebraic Curves and Their Period Matrices, *J. Symb. Comp.* **26**, 789 (1998).
- [15] E.ourgoulhon and S. Bonazzola, A formulation of the virial theorem in general relativity, *Class. Quant. Grav.* **11**, 443 (1994).
- [16] E.ourgoulhon, P. Haensel, R. Livine, E. Paluch, S. Bonazzola, and J.-A. Marck, Fast rotation of strange stars, *Astr. and Astrophysics*, **349** 851 (1999).
- [17] M. Heil, *Numerical Tools for the study of finite gap solutions of integrable systems*, PhD thesis, TU Berlin (1995).
- [18] M. Hoeij, An algorithm for computing an integral basis in an algebraic function field, *J. Symb. Comput.* **18**, 353 (1994).
- [19] A.R. Its, V.B. Matveev, Schrödinger operators with finite-gap spectrum and N-soliton solutions of Korteweg-de Vries equation, *Theor. Math. Physics* **23** (1), 51-67 (1975)
- [20] C. Klein and O. Richter, On a class of physically realistic solutions to the Ernst equation, *Phys. Rev. Lett.*, **79**, 565 (1997).
- [21] C. Klein and O. Richter, Physically realistic solutions to the Ernst equation on hyperelliptic Riemann surfaces, *Phys. Rev. D*, **58**, CID 124018 (1998).
- [22] C. Klein and O. Richter, Exact relativistic gravitational field of a stationary counter-rotating dust disk, *Phys. Rev. Lett.* **83**, 2884 (1999).
- [23] C. Klein, Exact relativistic treatment of stationary counter-rotating dust disks: boundary value problems and solutions, *Phys. Rev. D*, **63** 64033 (2001).
- [24] A. Komar, 'Covariant Conservation Laws in General Relativity', *Phys. Rev.*, **113**, 934 (1959).
- [25] D. Korotkin, Finite-gap solutions of the stationary axisymmetric Einstein equation, *Theor. Math. Phys.* **77** 1018-1031 (1989)
- [26] D. Korotkin and V. Matveev, Theta Function Solutions of the Schlesinger System and the Ernst Equation, *Funct. Anal. Appl.*, **34** 1 (2000).
- [27] D. Kramer, H. Stephani, E. Herlt and M. MacCallum, *Exact Solutions of Einstein's Field Equations*, Cambridge: CUP (1980).
- [28] I.M. Krichever, *Russ. Math. Surveys*, **44** No.32 144-225 (1989).
- [29] D. Maison, Are the stationary axially symmetric Einstein equations completely integrable?, *Phys. Rev. Lett.* **41** (1978) 521-524.
- [30] G. Neugebauer, R. Meinel, General relativistic gravitational field of the rigidly rotating disk of dust: Solution in terms of ultrahyperelliptic functions, *Phys. Rev. Lett.* **75** 3046-3048 (1995)
- [31] U. Schaudt, On the Dirichlet problem for the stationary and axisymmetric Einstein equations, *Comm. Math. Phys.*, **190**, 509, (1998).
- [32] M. Seppälä, Computation of period matrices of real algebraic curves, *Discrete Comput. Geom.* **11**, 65 (1994).



- [33] C.L. Tretkoff and M.D. Tretkoff, Combinatorial group theory, Riemann surfaces and differential equations, *Contemp. Math.* **33**, 467 (1984).
- [34] R. Wald, *General Relativity*, Chicago, London: The University of Chicago Press (1984).
- [35] [www.lorene.obspm.fr](http://www.lorene.obspm.fr)
- [36] [www-sfb288.math.tu-berlin.de/~jtem/](http://www-sfb288.math.tu-berlin.de/~jtem/)

INSTITUT FÜR ASTRONOMIE UND ASTROPHYSIK, UNIVERSITÄT TÜBINGEN, AUF DER MORGENSTELLE  
10, 72076 TÜBINGEN, GERMANY

*E-mail address:* [joergf@tat.physik.uni-tuebingen.de](mailto:joergf@tat.physik.uni-tuebingen.de)

LUTH, OBSERVATOIRE DE PARIS, 92195 MEUDON CEDEX, FRANCE

*Current address:* Max-Planck-Institut für Physik, Föhringer Ring 6, 80805 München, Germany

*E-mail address:* [klein@mppmu.mpg.de](mailto:klein@mppmu.mpg.de)

